Shape effect of hot droplets on fragmentation

Nobuyoshi Komatsu[1,*] and Takashi Abe[1,2,†]
[1]*Department of Aeronautics and Astronautics, University of Tokyo, Hongo 7-3-1, Bunkyo-ku, Tokyo, Japan*
[2]*The Institute of Space and Astronautical Science, Yoshinodai 3-1-1, Sagamihara, Kanagawa, Japan*
(Received 29 November 2004; revised manuscript received 17 March 2005; published 3 August 2005)

Fragmentation dynamics and the shape effect of initial hot droplets on it are investigated by using a classical molecular dynamics method. As the initial conditions for the fragmentation simulation, small hot droplets in the supercritical phase, with the number of particles N less than $\sim 10^3$, are considered. It is revealed that, in the process of the fragmentation, the largest cluster approaches a certain quasistable state corresponding to the so-called triple point. It is also revealed that the initial shape of the hot droplets has a significant effect on the cluster distribution generated after fragmentation; i.e., the more prolate the initial shape, the more markedly the size of the largest cluster decreases and the number of small clusters increases. The shape effect diminishes with an increasing number of particles in the initial hot droplet and could be negligible for large hot droplets, of the number of particles N more than $\sim 10^3$.

DOI: 10.1103/PhysRevE.72.021601 PACS number(s): 68.03.Fg, 36.40.Qv, 64.70.−p, 02.70.Ns

I. INTRODUCTION

Nanoscale materials composed of less than several thousands of atoms or molecules are called a "cluster" or a "nanocluster", and have attracted much attention from many researchers since their properties are quite different from those of corresponding bulk materials. For example, for argon clusters, *icosahedral* structures are known to be the most stable in contrast to cubic-close-packed lattice structures for bulk materials [1–5]. Historically, research into clusters started from the middle of the 20th century; in 1956, Becker *et al.* [6] studied the formation of clusters through the condensation of vapor expanding into a vacuum [7]. Since then, the unique properties of clusters such as geometrical structures, electronic structures, and dynamics have been extensively investigated because they have many applications in technological fields (e.g. nanomaterial designs, engine development, semiconductor manufacturing, etc.) [1,2].

In order to examine the formation process of these clusters, a "fragmentation" process (i.e., expansion of high-pressure droplets *in* a vacuum) has been widely studied [8–22]. In those works, molecular dynamics (MD) simulations have played an important role in analyzing the fragmentation process. This is because the fragmentation process is in a highly nonequilibrium state and is difficult to analyze theoretically [8].

By means of these MD simulations, various characteristics of the produced clusters such as the mean cluster size and the distribution of clusters have been investigated [8–21]. However, in most fragmentation simulations made in the past, the initial hot droplet was assumed to have a spherical configuration [8–15]. Even in the continuum-model study, a similar assumption was made for simplicity [22]. However we must be reminded that, in the supercritical phase for the initial droplet, the shape of the droplets can change without constraint since the surface tension will vanish. Therefore, we conclude that, in the previous studies, the initial hot droplets were unnecessarily assumed to have a spherical configuration. In fact, the shape of the hot droplets may deviate from the spherical configuration due to an external force or disturbance. Nevertheless, the effect of the shape (hereafter *shape effect*) on the fragmentation has not yet been investigated except in a few studies on evaporation [23–27]. However, it is expected that the initial shape has an influence on the fragmentation process since, in general, atoms residing in the surface layer of small clusters have a strong influence on the cluster behavior [1]. Therefore, in order to acquire a deeper understanding of the fragmentation process, it is necessary to evaluate the shape effect of the initial hot droplets. We will evaluate this in the present paper.

The present paper is organized as follows. In Sec. II, we give a brief review of the MD techniques to simulate the fragmentation process. In Sec. III, the initial conditions for the simulation are defined. In Sec. IV, we introduce several parameters such as the cluster distribution and temperature. In Sec. V, the simulation results are presented: In Sec. V A, we give an overview of the fragmentation process in relation to the dynamics of the largest cluster. In Sec. V B, the shape effect of initial hot droplets is investigated by using small droplets composed of less than $\sim 10^3$ particles. In Sec. V C, the size dependence of the shape effect is discussed for the droplets including the case of the number of particles up to the order of 10^3. Finally, the conclusion is given.

II. MD TECHNIQUES

For the fragmentation simulation, we integrate the set of classical equations of motion for the particles interacting through the following *shifted-force* potential U_{sf} or corresponding force F_{sf} [28]: for $r \leqslant r_{\mathrm{c}}$

$$U_{\mathrm{sf}}(r) = U_{\mathrm{LJ}}(r) - U_{\mathrm{LJ}}(r_{\mathrm{c}}) - [r - r_{\mathrm{c}}]\left(\frac{dU_{\mathrm{LJ}}}{dr}\right)_{r_{\mathrm{c}}}, \qquad (1)$$

*Present affiliation: The Institute of Space and Astronautical Science. E-mail address: n-komatsu@gd.isas.jaxa.jp
†E-mail address: tabe@gd.isas.jaxa.jp

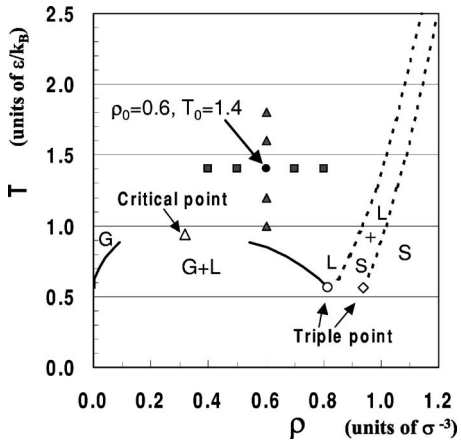

FIG. 1. Phase diagram for the shifted-force system. The open-triangle, -circle, and -diamond represent the vapor-liquid critical point, and the saturated liquid and solid phases at the triple point, respectively. G, L, and S represent the gas phase, the liquid phase, and the solid phase, respectively. The closed-circle, -triangles, and -squares represent the initial conditions for the simulation in this study. The phase diagram is cited from the Errington *et al.* work [29].

$$F_{\mathrm{sf}}(r) = -\left(\frac{dU_{\mathrm{LJ}}}{dr}\right) + \left(\frac{dU_{\mathrm{LJ}}}{dr}\right)_{r_c}, \tag{2}$$

$$U_{\mathrm{LJ}}(r) = 4\varepsilon\left[\left(\frac{\sigma}{r}\right)^{12} - \left(\frac{\sigma}{r}\right)^{6}\right], \tag{3}$$

while, for $r > r_c, U_{\mathrm{sf}}(r) = F_{\mathrm{sf}}(r) = 0$ is assumed. In the present study, the cut-off distance r_c is set to be 2.5σ. The constants, $\sigma, \varepsilon, m, \varepsilon/\kappa_B, \sigma(m/\varepsilon)^{1/2}$ are chosen, respectively, with units of length, energy, mass, temperature, and time, where κ_B is Boltzmann's constant. The set of equations of motion is integrated by using Verlet's algorithm with $\Delta t = 0.005\ \sigma(m/\varepsilon)^{1/2}$ as the time increment for the integration. For the present simulation of the fragmentation process, the total number of time steps is set to 40 000; i.e., the final time is $t = 200$.

In order to see the characteristics of the shifted-force potential system, we show the phase diagram of the simulated system in the $\rho - T$ plane (cited from the Errington *et al.* work [29]). In Fig. 1, the solid and dashed lines represent the vapor-liquid and liquid-solid phase boundaries, respectively. Above the bell-shaped vapor-liquid boundary, there is one single fluid phase called the supercritical phase. It should be noted that this phase diagram is applicable to bulk matter. In other words, the phase diagram does not precisely represent the state of the clusters because such sharp phase boundaries do not exist for the clusters. However, since the phase diagram for the bulk matter is useful to represent the *outline* of the behavior of the cluster, we refer to this phase diagram in the present study. Note that the properties of the clusters depend on the cut-off distance and the potential. However, we have confirmed that the main results in the present study are qualitatively universal even if the properties of the clusters are influenced by long-range forces, e.g., $r_c = 4\sigma$.

III. INITIAL CONDITIONS

A. Initial hot droplet

For the fragmentation simulations, an initial hot droplet must be prepared. To this aim, several methods have been proposed in MD simulations. For example, the initial droplet can be prepared by using a spherical wall within which the particles are confined [8,10]. In another method, it can be prepared by cutting out a spherical droplet from a thermally equilibrated periodic system [9,13,14]. In the present study, we employ the latter method because it is the simplest and the most suitable for our simulations. Moreover, it is well-known that the latter method is consistent with real experiments [18]. In the present paper, the initial hot droplet is prepared as follows:

• **Step I**: In a cubical cell, N_{eq} particles are equilibrated under periodic boundary conditions at a target temperature and number density. In the periodic system, the temperature is controlled by scaling of the velocities [30]. That is, the velocity of each particle with respect to a laboratory-fixed coordinate system $\mathbf{v}_i(t)$ is scaled simultaneously at an arbitrary instant time t by a common factor θ as

$$\mathbf{v}_i(t) \rightarrow \theta \mathbf{v}_i(t), \tag{4}$$

$$\theta = 1 + \alpha\left[\sqrt{\frac{T_b}{T(t)}} - 1\right], \tag{5}$$

where $T(t)$ is the instantaneous temperature of the system, and T_b is the temperature of the "cold heat-bath" (i.e., the target temperature) [30]. In the present simulation, the constant α is set to be 0.1. During this temperature control, the thermodynamic quantities approximately approach their equilibrium values. After reaching equilibrium, the temperature control is turned off, and the simulation is continued as a microcanonical ensemble simulation for at least 200 time steps, in order to obtain the equilibrium state for the initial droplets. It is confirmed, by Boltzmann's H function, that the system approaches the equilibrium state at the target temperature. We employed the above equilibrated system as the source for the initial droplets. In the present simulation, the number of particles in the equilibrated periodic system is approximately 20 000 ($N_{\mathrm{eq}} = 19\,652$).

• **Step II**: The initial droplets are generated by cutting out N particles from the inner region of an arbitrary physical shape within this equilibrated system. The cutting-out process is conducted as follows: The geometric configuration of arbitrary physical shape is projected into the equilibrated system randomly, and the particles inside the geometric configuration are selected for the potential droplet. From those selected droplets, the droplet that includes N particles is employed as the initial droplet. In such a way, these operations produce hot droplets at the target temperature, number density, and shape. The shape and the size of the initial droplet is described in Secs. III B and III C, respectively.

• **Step III**: As an initial setup for the simulation, the initial droplet thus obtained is put into a free space which is free from the periodic boundary conditions. Then, the MD calculation is carried out for the fragmentation simulation under

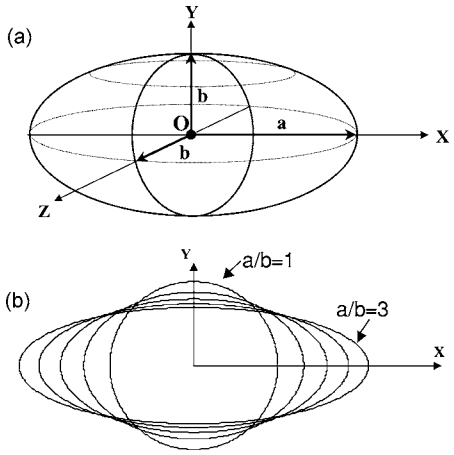

FIG. 2. Shape definition of droplets: (a) Sketch of shape of ellipsoid, (b) the sphere ($a/b=1$) and a family of ellipsoids ($a/b=1.5\sim3.0$) in the X-Y plane.

constant energy, i.e., the microcanonical ensemble simulation starts.

It should be noted that, under certain conditions such as a rarefied environment, high-angular momentum may generate an oblate spheroidal cluster (e.g., clusters in low-density environments, some galaxies [31], etc). Generally, high-angular momentum has a strong effect on the formation of clusters [32,33] (In the late 1980's and the early 1990's, Jellinek and Li investigated such structural properties and angular-momentum-driven isomerizations [34–36].). Therefore, in order to study the shape effect clearly, we will focus on *rotationless* initial droplets in the present paper. Nevertheless, we may obtain the droplet with very small angular momentum from the thermally equilibrated system. Therefore, in the present simulation, the velocities of the particles in the initial droplet are slightly modified in order to keep the total momentum and the total angular momentum as 0. The velocities of the particles in the droplet are modified as follows: For a droplet which is cut out from the equilibrated system, the angular momentum of the droplet is given by

$$\Delta\hat{\mathbf{L}} = \hat{\mathbf{I}} \cdot \Delta\hat{\boldsymbol{\omega}}, \tag{6}$$

where $\hat{\mathbf{I}}$ and $\Delta\hat{\boldsymbol{\omega}}$ represent the tensor of inertia and angular velocity of the droplet, respectively. The *hat* symbol (^) means that the quantity is defined in a coordinate system fixed with a droplet (which is shown in Fig. 2 in the next section). In order to cancel out the above angular momentum, the velocity of the ith particle in the droplet $\hat{\mathbf{v}}_i$ is modified as

$$\hat{\mathbf{v}}_i^{\text{mod.}} = \hat{\mathbf{v}}_i - \hat{\mathbf{r}}_i \times \Delta\hat{\boldsymbol{\omega}}, \tag{7}$$

where $\hat{\mathbf{r}}_i$ is a vector that locates the particle. Then, all the velocities of the particles are modified so that the total momentum of the droplet becomes 0. By means of these operations, we prepared a rotationless initial hot-droplet for the fragmentation simulation. Although these operations slightly affect the average temperature in the droplet, the variation in the temperature is less than 1% in the present study and it is confirmed that the above operations do not influence our main results.

B. Shape

In order to investigate the shape effect of the initial droplet, it is necessary to define a shape suitable for our study. For instance, Celestini and Bosch [24] and Celestini *et al.* [25] investigated the shape dependence on the melting temperature by using ellipsoidal clusters and cylindrical clusters. Mareschal *et al.* [26] and Bardouni [27] have investigated the shape-dependence on the local pressure by using cylindrical interfaces and planar interfaces to study the liquid-vapor interfaces. In the present paper, we consider the following ellipsoid for simplicity:

$$\frac{x^2}{a^2} + \frac{y^2}{b^2} + \frac{z^2}{b^2} \leqslant 1 \quad (a \geqslant b), \tag{8}$$

where, as shown in Fig. 2(a), a and b are the semimajor axis and semiminor axis, respectively. That is, $a/b=1$ represents a sphere. Accordingly, the larger a/b is, the more prolate the shape is, as shown in Fig. 2(b). Note that, in the following, a/b is referred to as the *flatness ratio*.

In the present simulation, we determine the configuration of the initial droplet as follows. First, we specify the number of particles in the droplet N, the flatness ratio a/b, and the initial number density ρ_0 at the equilibrated system in Step I, Sec. III A. Here, the number of particles in the droplet N and the volume of the droplet V are defined as

$$N = \rho_0 V, \tag{9}$$

$$V = f(a,b). \tag{10}$$

Substituting Eq. (9) into Eq. (10) and solving Eq. (10) with respect to the flatness ratio a/b give a and b independently. For example, in the case of the sphere (i.e., $a/b=1$), the radius of the initial droplet $R_0(=a=b)$ is given by

$$R_0 = \left(\frac{N}{\frac{4}{3}\pi\rho_0} \right)^{1/3}. \tag{11}$$

Similarly, even in the case of the ellipsoid (i.e., $a/b>1$), a and b can be calculated.

C. Size of initial droplet

The properties of clusters composed of less than $\sim10^3$ particles are quite different from those of bulk materials [1,2]. This is because the influence of particles around the cluster's surface, i.e., "surface-effect," is not negligible. To anticipate this surface effect, we evaluate it for a droplet composed of N particles. Suppose that the radius of the droplet is R, and the number of particles in the surface layer is N_{sur}, then N_{sur} and N would be approximately proportional to the surface area ($\sim R^2$) and its volume ($\sim R^3$), respectively. Since the influence of the surface of the droplet is related to the number of particles in the surface layer, the surface effect can be evaluated as

$$\frac{N_{\mathrm{sur}}}{N} \propto \frac{R^2}{R^3} = \frac{1}{R} \propto \frac{1}{N^{1/3}}. \tag{12}$$

Equation (12) tells us that, with decreasing N, the relative influence of the particles in the surface layer increases. In other words, since the shape of the droplet directly affects the surface area, it is expected that the shape effect increases with decreasing N. In this context, small droplets would be suitable for examining the shape effect because of the larger surface effect. Therefore, in the present paper, the number of particles in the small droplet was set to be $N=160$ as a typical value. Moreover, in order to study the size dependence, the system size was varied in the range from $N=160$ to $N=1060$.

D. Initial density and temperature of the droplet

In order to investigate the fragmentation process properly, typical values for the initial number density and system temperature were chosen as $\rho_0=0.6$ and $T_0=1.4$, respectively. As shown in Fig. 1, the typical initial condition $(\rho_0, T_0)=(0.6, 1.4)$ is in the supercritical phase (As mentioned previously, we refer to the phase diagram for *bulk matter* although it does not precisely represent the state of the clusters.). Its temperature is approximately one and one half times larger than the critical temperature, and its number density is approximately in the middle between the critical density and the density at the triple point for the saturated liquid. Hereafter, we refer to the typical initial condition $(\rho_0, T_0)=(0.6, 1.4)$ as "the standard initial condition."

The present standard initial condition is suitable for our simulation since, for $T_0 \gg 1.4$, too many small clusters are generated during the simulation and the largest cluster becomes too small. On the other hand, for $T_0 \ll 1.4$, any clusters are hardly generated. In this study, since we also discuss the temperature effect and the number density effect, we have selected the following initial conditions:

(1) The standard initial condition: $\rho_0=0.6, T_0=1.4$

(2) For the temperature effect: $\rho_0=0.6, T_0=1.0 \sim 1.8$ $(\Delta T_0=0.2)$

(3) For the number density effect: $\rho_0=0.4 \sim 0.8$, $T_0=1.4$ $(\Delta \rho_0=0.1)$

In Fig. 1, the above three conditions are represented as the closed circle, closed triangles, and closed squares, respectively. Note that, under identically prepared initial conditions, each simulation result is slightly different from the others due to statistical fluctuations. However, we have confirmed that averaging over 100 simulations is sufficient to see an averaged behavior. All the results in the present paper are averaged over 100 simulations with the identically prepared initial droplets.

IV. PARAMETERS FOR FRAGMENTATION ANALYSIS

In this section, in order to analyze the fragmentation phenomenon in the simulation, we will define several physical quantities such as the cluster distribution, temperature, and the number density of the largest cluster. It should be noted that all the physical quantities are averaged over 100 simulations with identically prepared initial droplets.

A. Definition of cluster and its distribution

First of all, we define a cluster as a group of particles which satisfy the following condition. That is, for any particle in the group, the ith particle can find the nearest neighbor, the jth particle, satisfying the following constraint:

$$|\mathbf{r}_i - \mathbf{r}_j| \leqslant r_{\mathrm{cl}}, \tag{13}$$

where r_{cl} is a parameter called a clusterization radius [15]. This definition has been widely used in previous studies [8,9,17–19]. In the present study, the clusterization radius is set to be $r_{\mathrm{cl}}=2.5\sigma$, which corresponds to the value of the potential cut-off distance r_{c}. Note that our simulation results are not affected much even if we set r_{cl} to be 2.3σ.

Now that once the cluster is defined, we can define a distribution of the cluster size $N_c(n)$ where $N_c(n)$ represents the number of clusters with size equal to n particles. According to the distribution, we define a cumulative number of clusters $C(n)$ as

$$C(n) = \sum_{i=n+1}^{N_{\mathrm{Cmax}}} N_c(i) \quad (n \geqslant 1), \tag{14}$$

where N_{Cmax} is the number of particles in the largest cluster. In other words, $C(n)$ is the cumulative number of clusters with size greater than n particles. Note that $C(n)$ does not contain the number of monomers $N_c(1)$.

In this paper, we employ the cumulative number $C(n)$ for our analysis, instead of $N_c(n)$. This is because $N_c(n)$ fluctuates largely in a statistical sense, especially for large n. Hereafter we call $C(n)$ the cluster distribution.

B. Temperatures

In the fragmentation process, the center-of-mass velocity of each cluster is not necessarily equal to 0, although the total momentum of the system is kept as 0. Thus, it is necessary to define an internal temperature for each cluster, taking into account the center-of-mass motion of each cluster. First of all, we define the internal temperature for the "n cluster," i.e., the cluster of size n. According to the Ikeshoji *et al.* work [3], the internal temperature for the n-cluster $T_{\mathrm{inn}}(n)$ is defined as

$$T_{\mathrm{inn}}(n) = \frac{m}{3(n-1)N_n k_B} \sum_{j=1}^{N_n} \sum_{i=1}^{n} (\mathbf{v}_{i,j} - \bar{\mathbf{V}}_j)^2, \tag{15}$$

where N_n is the number of n clusters [i.e., $N_c(n)$], and $\mathbf{v}_{i,j}$ is the velocity of the particle i in cluster j (with respect to a laboratory-fixed set of coordinate axes). The center-of-mass velocity $\bar{\mathbf{V}}_j$ of each cluster j containing n particles is given by

$$\bar{\mathbf{V}}_j = \frac{1}{n} \sum_{i=1}^{n} \mathbf{v}_{i,j}. \tag{16}$$

By using the internal temperature for the n cluster, we define the averaged internal temperature of the system $T_{\mathrm{inn}}^{\mathrm{sys}}$ as

$$T_{\mathrm{inn}}^{\mathrm{sys}} = \frac{1}{\sum_{n=2}^{\infty}(n-1)N_n}\sum_{n=2}^{\infty}(n-1)T_{\mathrm{inn}}(n). \tag{17}$$

In other words, $T_{\mathrm{inn}}^{\mathrm{sys}}$ corresponds to the averaged thermal temperature of the system. In the present paper, we do not discuss the rotational temperature of the cluster because it is relatively small [8,19].

C. Number density of the largest cluster

During the fragmentation process, we can find the largest cluster at each instant. Unlike recent studies on the fragmentation process, which were focused on the cluster distribution, we will discuss the behavior of the largest cluster as well. This is because the fragmentation process is a kind of evaporation process, if one cluster is much larger than the others, so we can discuss the fragmentation behavior referring to the knowledge accumulated for the evaporation process.

To see the behavior of the largest cluster, its internal temperature and number density are analyzed in the present paper. For the number density of the largest cluster, we define a new quantity, the *averaged number density* as

$$\rho_{\mathrm{ave}}(N_{\mathrm{Cmax}}) = \frac{N_{\mathrm{Cmax}}}{\frac{4}{3}\pi\bar{r}^3}, \tag{18}$$

$$\bar{r} = \frac{4}{3}\frac{\sum_{i=1}^{N_{\mathrm{Cmax}}} r_{\mathrm{c.m},i}}{N_{\mathrm{Cmax}}}, \tag{19}$$

where $r_{\mathrm{c.m},i}$ is the distance of particle i from the center of mass of the largest cluster [9]. We must keep in mind that the number density defined in Eq. (18) is an averaged one, although the local density of the largest cluster is expected to be inhomogeneous [37]; that is, its number density may vary from location to location. Note that the averaged number density thus defined is determined at each instant and varies with time.

V. RESULTS

In this section, all results represent those averaged over 100 simulations with identically prepared initial droplets, and the error bars in some figures indicate the reliability of 68% confidence level in terms of the normal error distribution.

A. Fragmentation process and the largest cluster

By means of the MD simulation, we can now study the shape effect of initial hot droplets on fragmentation. Before proceeding further, however, it is appropriate to describe the fragmentation behavior commonly observed in the present simulation. For this purpose, in this section, we present, as a typical result, the case for the *spherical* hot droplets under the standard initial condition, $(\rho_0, T_0)=(0.6, 1.4)$.

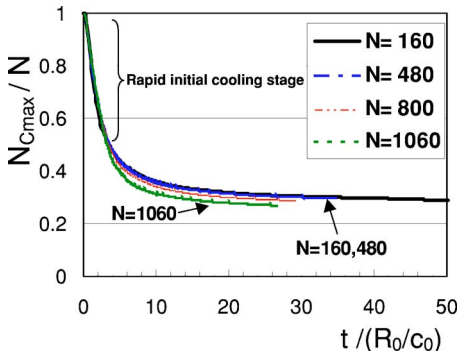

FIG. 3. (Color online) Normalized time evolution of N_{Cmax}. Each simulation starts from the standard initial condition $(\rho_0, T_0)=(0.6, 1.4)$. The horizontal axis indicates a nondimensional time.

In the fragmentation process, the initial hot droplet expands rapidly and begins breaking up into many clusters as soon as the simulation starts. To illustrate this, we will focus on the behavior of the largest cluster at each instant observing its time evolution for initial droplets of various sizes. As shown in Fig. 3, the size of the largest cluster N_{Cmax} decreases rapidly. This first stage corresponds to an adiabatic-like expansion and is called the "*rapid initial cooling stage*" [10]. Note that, in the figure, the vertical axis is normalized by N, and the horizontal axis is normalized by R_0/c_0 [8]. Here, c_0 and R_0 are the sound speed in the initial hot droplet and its initial radius, respectively. For example, from Eq. (11), the radius R_0 of the spherical initial droplet of 160 particles is approximately 3.99σ.

After the first stage, each curve of N_{Cmax}/N decreases slowly, and finally approaches a quasisteady state. The behavior of each curve is quite consistent, especially during the rapid initial cooling stage, even though the droplet size ranges from 160 to 1060. From this fact, it is expected that the behavior of the fragmentation process is well characterized by the system size N, the sound speed of the initial droplet c_0, and the initial radius R_0. Note that the size of the largest cluster increases with the size of the initial hot droplet.

Next, we observe the evolution of the largest cluster in the $\rho-T$ plane and discuss it referring to the phase diagram for bulk matter. It should be noted that the phase diagram refers to a macroscopic system and thus it may not be appropriate to discuss the state of the present small cluster since, as pointed out previously, such sharp phase boundaries do not exist for the clusters. Furthermore, we must be reminded that the number density of the cluster is defined as an *average*, neglecting the inhomogeneities in the largest cluster. Nevertheless, the following discussion is useful to understand the *outline* of the behavior of the largest cluster in the fragmentation process. The evolution of the largest cluster in the $\rho-T$ plane is shown for the standard initial conditions with various initial sizes in Fig. 4(a) and for the other initial conditions with $N=160$ in Fig. 4(b). In these figures, the closed-marks represent the initial conditions described in Sec. III D, and each path of the largest cluster starts from each initial condition. The closed circle indicates the standard initial condition $(\rho_0, T_0)=(0.6, 1.4)$. During the rapid initial cooling

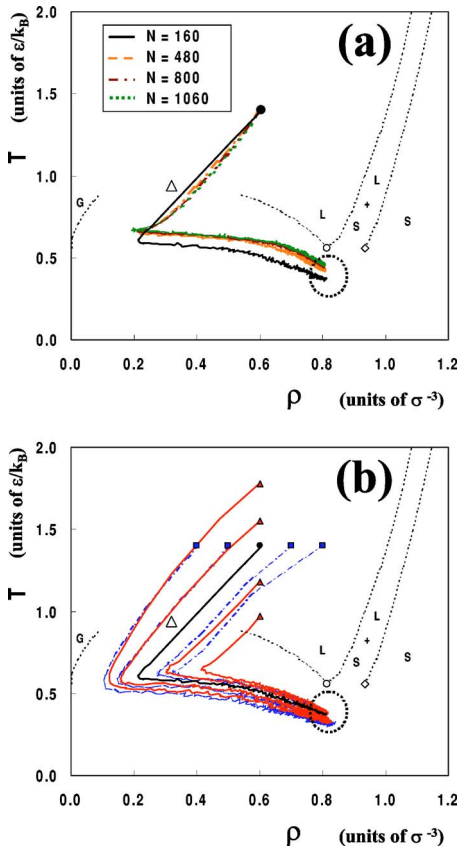

FIG. 4. (Color online) Path of the largest cluster in the $\rho-T$ plane. (a) The droplet size N is varied from 160 to 1060 under the standard initial condition. (b) The initial condition, i.e., the initial temperature or the initial number density, is varied with $N=160$.

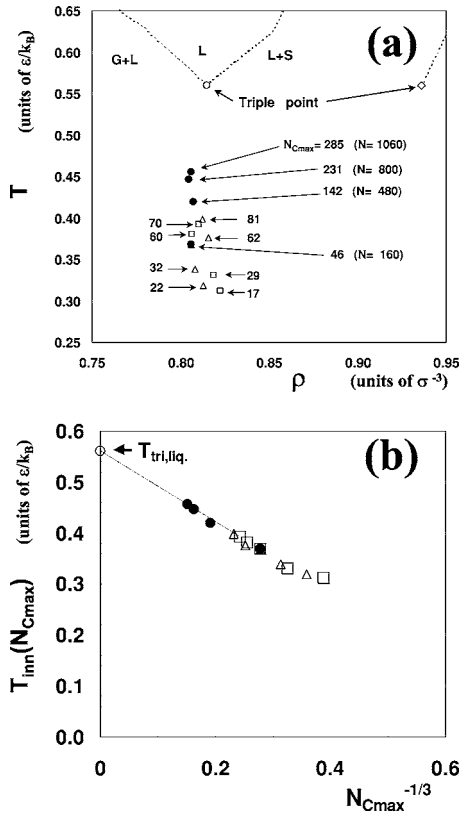

FIG. 5. The largest cluster in the final quasistable state. (a) Property of the largest cluster in the $\rho-T$ plane. (b) Internal temperature of the largest cluster as a function of $(N_{\mathrm{Cmax}})^{-1/3}$. The final quasistable states in Fig. 4(a) are replotted as the closed circles (●). The open triangles (△) and squares (□) indicate the final states obtained from the simulations for the temperature effect and the number density effect, respectively, which appear in Fig. 4(b).

stage, both the temperature and the number density of the largest cluster decrease. This behavior of the fragmentation is similar to that of adiabatic-like expansion although each behavior is slightly different from each other [38]. The cause of this expansion is due to the fact that, initially, the surface tension would vanish since the state of the initial droplet is in the supercritical phase; i.e., above the bell-shaped vapor-liquid coexistence curve. The general behavior of the largest cluster determined from the present study agrees well with the results in Refs. [8,9]. Because of this expansion, the internal temperature decreases to a certain value near the vapor-solid phase boundary in the vapor-liquid phase and simultaneously, the density approaches the minimum value. Since this state is in the vapor-liquid phase, the surface tension would arise. Because of this surface tension, after reaching the lowest density, the largest cluster starts to shrink gradually and approaches a certain state. Note that the temperature of the largest cluster, when its number density approaches the minimum value, is almost common to each path.

As shown in the same figures, all the paths finally approach their quasistable states, as highlighted by the dotted circles. That is, all the fragmentation processes end with the formation of the clusters in the quasistable state. Note that this quasistable cluster can exist even under vacuum conditions although, under vacuum conditions, bulk materials can evaporate at any temperature. This is because the small cluster has a non-negligible energy threshold below which evaporation cannot take place, while the bulk material always has sufficient energy to overcome the energy-barrier corresponding to the single-atom evaporation at any temperature (e.g., the bulk material is usually in a heat bath). A similar behavior of the fragmentation process was reported in Ref. [10], however, the characteristics of the cluster in the final quasistable state were not investigated and remained an open question.

The final quasistable states appearing in Fig. 4(a) and 4(b) are replotted in Fig. 5(a). The number with an arrow shown in Fig. 5(a) indicates the size of the largest cluster N_{Cmax} in the final state. First it should be noticed that the final quasistable states scatter near the triple point showing a good correlation with the final cluster size. As a matter of fact, the final quasistable clusters have various sizes depending on the initial conditions. For example, the size of the final largest cluster derived from the standard initial condition with various initial sizes increases with the initial hot-droplet size N, as shown in Fig. 5(a) and (Fig. 3). In the final state, the smaller the cluster size, the lower its temperature becomes. Conversely, the larger the cluster size in the final state, the more closely its state approaches the triple point. Taking into

account the fact that the temperature of the triple point is defined for bulk matter, it is expected that the finite size effect suggested in Ref. [39] may explain this temperature departure from the triple point (In the early 20th century, Rayleigh discussed a similar size effect from a viewpoint of hydrodynamics; i.e., vapor pressure of small particles [40].). For example, it has been shown, by the MD simulation in a homogeneous system with periodic boundary conditions, that the temperature of the vapor-liquid phase boundary decreases with decreasing the system size [41]. More precisely, it has also been pointed out that the melting point of clusters decreases in proportion to $N_{\mathrm{cl}}^{-1/3}$, with a decreasing number of particles in the cluster N_{cl} [42,43]. Since these simulation results were obtained from the equilibrium states, these conclusions may not be applicable to the fragmentation simulation. However, suppose that they are applicable to the present case, it is expected that the final states of the largest cluster are related to the triple point near which all the final states reside.

To confirm this explanation, we plot the internal temperature of the largest cluster in the final state, as a function of $(N_{\mathrm{Cmax}})^{-1/3}$. Note that, since we focus only on the largest cluster, we employ N_{Cmax} instead of N_{cl} hereafter. As shown in Fig. 5(b), the internal temperature of the largest cluster decreases in proportion to $(N_{\mathrm{Cmax}})^{-1/3}$. In the limit of an extremely large N_{Cmax}, the internal temperature becomes quite consistent with the temperature at the "so-called" triple point $T_{\mathrm{tri,liq}}$, as indicated by the extension of the line from the simulation results. Accordingly, it may be concluded that the internal temperature of each of the largest clusters approaches a certain temperature corresponding to the triple point. Similarly, as shown in Fig. 5(a), the averaged number density of the largest cluster also seems to approach the number density at the triple point. Even though the present result described here is for an initially spherical droplet, we have obtained the same result not only for the initially *ellipsoidal* droplet but also for other initial conditions, e.g., $(\rho_0, T_0) = (0.6, 3.0)$ [38]. Note that since the approach to the triple point is an empirical observation, a comprehensive theory on this behavior cannot be given here. However, the present simulation results suggest that the largest cluster approaches a certain quasistable state corresponding to the so-called triple point.

B. Shape effect of small droplets

In order to investigate the shape effect, the initial shape is varied from $a/b=1$ to $a/b=3$ under the standard initial conditions $(\rho_0, T_0)=(0.6, 1.4)$. In this section, the droplet size is set to be $N=160$ because the small droplet is more suitable for studying the shape effect clearly.

First, we will investigate the behavior of the number of particles in the largest cluster. As described in the previous section and shown in Fig. 6(a), the number of particles in the largest cluster N_{Cmax} decreases rapidly. After the rapid initial cooling stage, N_{Cmax} decreases slowly, and finally approaches a quasisteady state. This general behavior is universal in every case, however, N_{Cmax} at each instant depends upon the flatness ratio a/b. Especially after the rapid initial cooling

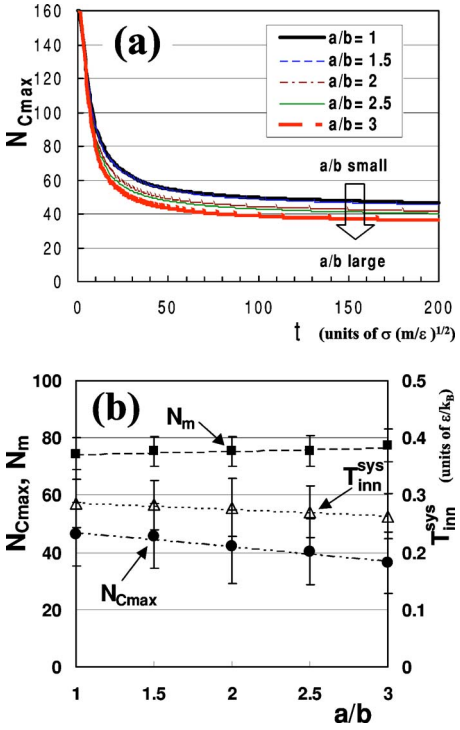

FIG. 6. (Color online) Shape effect of small droplets. (a) Time evolution of N_{Cmax}. (b) Typical physical quantities at the final time $(N_{\mathrm{Cmax}}, N_{\mathrm{m}}, T_{\mathrm{inn}}^{\mathrm{sys}})$. The error bars indicate the reliability of 68% confidence level in terms of the normal error distribution.

stage, N_{Cmax} is quantitatively influenced by the variation of shape. In order to examine its effect clearly, we plot N_{Cmax} at the final time, against the flatness ratio a/b. As shown in Fig. 6(b), the larger the flatness ratio, the smaller N_{Cmax} becomes. To interpret the influence of the flatness ratio, we must be reminded that the size of the surface area depends on the flatness ratio; i.e., the surface area ratio with fixed volume is approximately proportional to the flatness ratio. Since the surface effect depends on the size of the surface area, it is expected that the influence of the flatness ratio appears through the size of the surface area. Based on this fact, we can reinterpret the present phenomenon as follows: The number of particles in the largest cluster decreases with increasing the surface area of the hot-droplet.

Next, we will focus on the behavior of the number of monomers N_{m}. As shown in Fig. 6(b), N_{m} increases with increasing flatness ratio. However, the increase rate of N_{m} is lower than the decrease rate of N_{Cmax}. Thus, it is expected that not only monomers but also small clusters increase in number, due to the increase in the flatness ratio a/b. In fact, as shown in Fig. 7(a), the cluster distribution $C(n)$ for larger n decreases with increasing a/b, while $C(n)$ for smaller n increases. In order to display this effect more clearly, we define the normalized cluster distribution as

$$C_R\left(\frac{n}{N_{\mathrm{Cmax}}}\right) \equiv \frac{C(n:a/b=X)}{C(n:a/b=1)}, \tag{20}$$

where X is an arbitrary value of the flatness ratio. Based on Eq. (20), we replot the normalized cluster distribution in Fig.

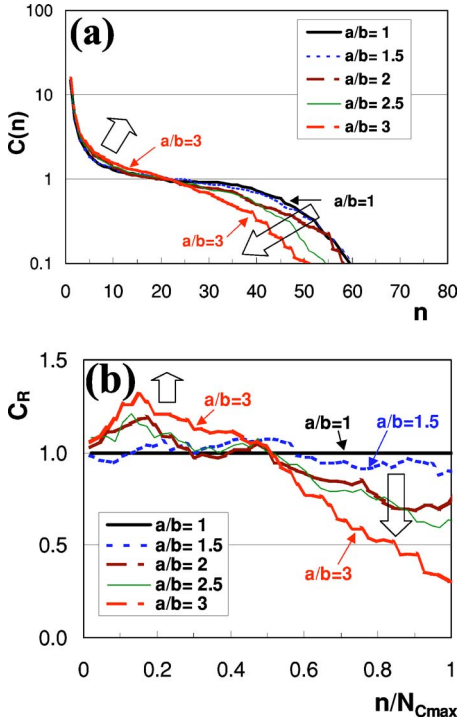

FIG. 7. (Color online) Shape effect. (a) Cluster distributions $C(n)$. (b) Normalized cluster distributions C_R. Each curve is averaged over 100 simulations with identically prepared initial droplets.

7(b). Note that, in this figure, although each curve is fluctuating, the uncertainty due to the fluctuations is small compared with variation in C_R along the curve. As shown in Fig. 7(b), the normalized cluster distribution C_R for $n/N_{\mathrm{Cmax}} \lessapprox 0.5$ increases with increasing flatness ratio a/b. On the other hand, $n/N_{\mathrm{Cmax}} \gtrapprox 0.5$, C_R decreases with increasing a/b. Therefore, it can be concluded that by increasing the flatness ratio or increasing the surface area, the number of large clusters decreases and that of small clusters increases.

So far, we have presented the results obtained for the standard initial condition $(\rho_0, T_0)=(0.6, 1.4)$. However, at least under various initial conditions in the supercritical phase, which are represented in Fig. 1, we can confirm a

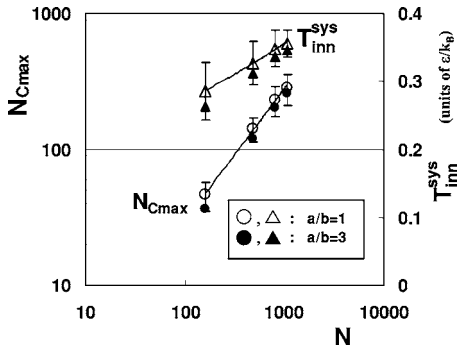

FIG. 8. Size dependence of the shape effect. The circles and triangles represent N_{Cmax} and $T_{\mathrm{inn}}^{\mathrm{sys}}$, respectively. The open marks and closed marks represent $a/b=1$ and $a/b=3$, respectively. The error bars indicate the reliability of 68% confidence level in terms of the normal error distribution.

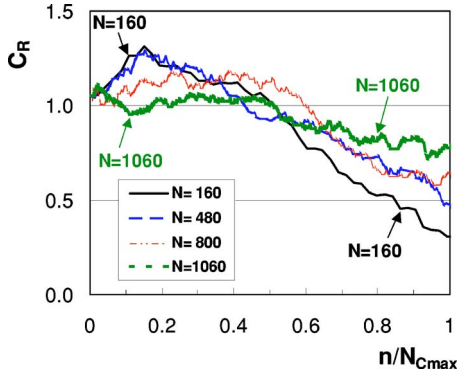

FIG. 9. (Color online) Size dependence of the shape effect.

shape effect similar to the present result [38]. Accordingly, we can conclude that the present shape effect appears under the initial conditions in the supercritical phase, at least near the standard initial condition.

C. Size dependence of the shape effect

Finally, we will discuss the size dependence of the shape effect. For this purpose, the system size is varied from $N=160$ to $N=1060$ under the standard initial condition, $(\rho_0, T_0)=(0.6, 1.4)$, while the flatness ratio a/b is set to be 1 or 3.

In order to investigate the size dependence of the shape effect, we examine N_{Cmax} and $T_{\mathrm{inn}}^{\mathrm{sys}}$ in the final state. As shown in Fig. 8, N_{Cmax} and $T_{\mathrm{inn}}^{\mathrm{sys}}$ in the final state increase with increasing system size N, however, the difference between the results for $a/b=1$ and $a/b=3$ decreases with increasing N. In other words, the shape effect diminishes with increasing system size N. This tendency can be also observed in the normalized cluster distribution C_R, as shown in Fig. 9. That is, for the larger droplet, the number of small clusters decreases and that of large clusters increases; as a result, the distribution of the larger droplet approaches that of the spherical initial droplet (i.e., $C_R=1$). Therefore, it is expected that the shape effect becomes negligible for larger droplets, from the viewpoint of the cluster distribution as well. This is reasonable because, as suggested in Eq. (12), the surface effect generally decreases in proportion to $N^{-1/3}$: Especially, the shape effect may be negligible in large systems of size more than the order of 10^3.

VI. CONCLUSION

In this paper, the fragmentation dynamics and the shape effect of the initial hot droplet were investigated by means of a molecular dynamics simulation. The hot droplet in the supercritical phase, with size N less than the order of 10^3, was considered as the initial condition for the fragmentation simulation. The largest cluster, which is generated during the fragmentation, approaches a certain quasistable state which is found to correspond to the so-called triple point defined for bulk matter. It is also found that the initial shape of the hot droplets has a significant effect on the fragmentation behavior; i.e., the more prolate the initial shape, the more

markedly the size of the largest cluster decreases and the number of small clusters increases. This shape effect appears due to the increase in the surface area since the more prolate the shape, the more markedly the surface area or the surface effect increases. The present shape effect diminishes with increasing number of particles in the initial hot droplet and could be negligible in the case of large hot droplets, of size N more than the order of 10^3.

[1] T. Kondow *et al.*, *Cluster, Selected papers in Physics X* (The Physics Society of Japan, Tokyo, 1997.
[2] H. Haberland, *Clusters of Atoms and Molecules I. Theory, Experiment, and Clusters of Atoms* (Springer-Verlag, Berlin 1995), 2nd ed.
[3] T. Ikeshoji *et al.*, J. Chem. Phys. **105**, 5126 (1996).
[4] T. Ikeshoji, B. Hafskjold, Y. Hashi, and Y. Kawazoe, Phys. Rev. Lett. **76**, 1792 (1996).
[5] T. Ikeshoji, G. Torchet, M. F. deFeraudy, and K. Koga, Phys. Rev. E **63**, 031101 (2001).
[6] E. W. Becker, K. Bier, and W. Henkes, Z. Phys. **146**, 333 (1956).
[7] O. F. Hagena, Rev. Sci. Instrum. **63**, 2374 (1992).
[8] J. A. Blink and W. G. Hoover, Phys. Rev. A **32**, 1027 (1985).
[9] A. Vicentini, G. Jacucci, and V. R. Pandharipande, Phys. Rev. C **31**, 1783 (1985).
[10] R. S. Dumont, S. Jain, and A. G. Basile, J. Chem. Phys. **102**, 4227 (1995).
[11] V. N. Kondratyev, H. O. Lutz, and S. Ayik, J. Chem. Phys. **106**, 7766 (1997).
[12] V. N. Kondratyev and H. O. Lutz, Z. Phys. D: At., Mol. Clusters **40**, 210 (1997).
[13] A. Strachan and C. O. Dorso, Phys. Rev. C **55**, 775 (1997).
[14] P. Balenzuela, C. A. Bonasera, and C. O. Dorso, Phys. Rev. E **62**, 7848 (2000).
[15] A. Chernomoretz, M. Ison, S. Ortiz, and C. O. Dorso, Phys. Rev. C **64**, 024606 (2001).
[16] X. Campi, H. Krivine, E. Plagnol, and N. Sator, Phys. Rev. C **67**, 044610 (2003).
[17] B. L. Holian and D. E. Grady, Phys. Rev. Lett. **60**, 1355 (1988).
[18] S. Toxvaerd, Phys. Rev. E **58**, 704 (1998).
[19] W. T. Ashurst and B. L. Holian, Phys. Rev. E **59**, 6742 (1999).
[20] W. T. Ashurst and B. L. Holian, J. Chem. Phys. **111**, 2842 (1999).
[21] S. Chikazumi and A. Iwamoto, Phys. Rev. C **65**, 067601 (2002).
[22] D. E. Grady, J. Appl. Phys. **53**, 322 (1982).
[23] L. Consolini, S. K. Aggarwal, and S. Murad, Int. J. Heat Mass Transfer **46**, 3179 (2003).
[24] F. Celestini and A. T. Bosch, Phys. Lett. A **207**, 307 (1995).
[25] F. Celestini *et al.*, Z. Phys. D: At., Mol. Clusters **37**, 49 (1996).
[26] M. Mareschal, M. Baus, and R. Lovett, J. Chem. Phys. **106**, 645 (1997).
[27] H. E. Bardouni *et al.*, J. Chem. Phys. **113**, 9804 (2000).
[28] J. J. Nicolas *et al.*, Mol. Phys. **37**, 1429 (1979).
[29] J. R. Errington, P. G. Debenedetti, and S. Torquato, J. Chem. Phys. **118**, 2256 (2003).
[30] M. Tanaka, J. Phys. Soc. Jpn. **51**, 3802 (1982).
[31] M. H. Jones, R. J. Lambourne, and D. J. Adams, *An Introduction to Galaxies and Cosmology* (Cambridge University, Cambridge, England, 2004).
[32] S. Weerasinghe and F. G. Amar, J. Chem. Phys. **98**, 4967 (1993).
[33] F. Calvo and P. Parneix, J. Chem. Phys. **119**, 256 (2003).
[34] J. Jellinek and D. H. Li, Phys. Rev. Lett. **62**, 241 (1989).
[35] D. H. Li and J. Jellinek, Z. Phys. D: At., Mol. Clusters **12**, 177 (1989).
[36] J. Jellinek and D. H. Li, Chem. Phys. Lett. **169**, 380 (1990).
[37] S. M. Thompson *et al.*, J. Chem. Phys. **81**, 530 (1984).
[38] N. Komatsu, Ph.D. thesis, University of Tokyo, 2004.
[39] D. Frenkel and B. Smit, *Understanding Molecular Simulation. From Algorithms to Applications* (Academic, San Diego, 2002).
[40] L. Rayleigh, Philos. Mag. **34**, 94 (1917).
[41] A. H. Raduta and A. R. Raduta, Nucl. Phys. A **724**, 233 (2003).
[42] A. Rytkönen, S. Valkealahti, and M. Manninen, J. Chem. Phys. **106**, 1888 (1997).
[43] A. Rytkönen, S. Valkealahti, and M. Manninen, J. Chem. Phys. **108**, 5826 (1998).